CD4+ T cell–mediated HLA class II cross-restriction in HIV controllers

Moran Galperin[1], Carine Farenc[2], Madhura Mukhopadhyay[1], Dhilshan Jayasinghe[2], Amandine Decroos[1], Daniela Benati[1], , Li Lynn Tan[2], Lisa Ciacchi[2], Hugh H. Reid[2,3], Jamie Rossjohn[2,3,4], Lisa A. Chakrabarti[1,5], and Stephanie Gras[2,3]

1 Pasteur Institute, Viral Pathogenesis Unit, Paris, France.
2 Infection and Immunity Program and Department of Biochemistry and Molecular Biology, Biomedicine Discovery Institute, Monash University, Clayton, Victoria 3800, Australia.
3 ARC Centre of Excellence in Advanced Molecular Imaging, Monash University, Clayton, Victoria 3800, Australia.
4 Institute of Infection and Immunity, School of Medicine, Cardiff University, Cardiff CF14 4XN, UK.
5 INSERM, U1108, Paris, France.

ABSTRACT

Rare individuals, termed HIV controllers, spontaneously control HIV infection by mounting efficient T cell responses against the virus. Protective $CD4^+$ T cell responses from HIV controllers involve high-affinity public T cell receptors (TCRs) recognizing an immunodominant capsid epitope (Gag293) presented by a remarkably broad array of human leukocyte antigen (HLA) class II molecules. Here, we determine the structures of a prototypical public TCR bound to HLA-DR1, HLA-DR11, and HLA-DR15 molecules presenting the Gag293 epitope. TCR recognition was driven by contacts with the Gag293 epitope, a feature that underpinned the extensive HLA cross-restriction. These high-affinity TCRs promoted mature immunological synapse formation and cytotoxic capacity in both $CD4^+$ and $CD8^+$ T cells. The public TCRs suppressed HIV replication in multiple genetic backgrounds ex vivo, emphasizing the functional advantage conferred by broad HLA class II cross-restriction

INTRODUCTION

Despite recent advances in antiretroviral therapy (ART) in controlling HIV-1 infection, HIV remains a major public health issue. Accordingly, there is a strong incentive to develop immunotherapeutic approaches to circumvent the need for lifelong ART, with the aim of achieving a functional HIV cure [1]. Because HIV-1 infection is primarily controlled by cell-mediated adaptive immunity, understanding how T cells detect HIV-1–infected cells is key for developing new immunotherapies and vaccines.

Most individuals succumb to HIV-1–related death in the absence of ART. However, some rare individuals, termed HIV controllers, spontaneously control HIV replication and avoid disease progression in the absence of ART. HIV controllers maintain low viral load and generally high $CD4^+$T cell numbers [2]. Human leukocyte antigen (HLA) genetics has been implicated in HIV-1 control, with some *HLA-I* alleles, including *HLA-B57*, *HLA-B27*, and *HLA-B81*, being associated with protection from HIV-1 disease progression [3–6]. This protection is attributable to specific $CD8^+$ T cells having superior functional properties, including efficient recognition of HIV-1 escape variants [5, 7–9]. Some protective HIV-1 $CD8^+$ T cell responses are associated with highly biased TCR gene usage, with particular T cell receptor (TCR) clonotypes accounting for potent effector T cell functions characteristic of HIV-1 control in asymptomatic $HLA\text{-}B57^+$ and/or $HLA\text{-}B27^+$ individuals [5, 7]. However, whether other immune mechanisms contribute to HIV-1 control remains unclear.

$CD4^+$ T cells also contribute to HIV-1 control [10–14], although their role in containing the virus remains poorly understood. Although HIV-infected $CD4^+$ T cells are rapidly depleted in HIV progressors, they persist and maintain high proliferative capacity in HIV controllers. Patients treated with ART can restore $CD4^+$ T cell levels over time, but only controller $CD4^+$ T cells can maintain advanced T helper 1 (T_H1) effector differentiation despite low levels of HIV-1 antigen [15, 16]. Although some HLA-II associations with HIV-1 control have been described, they are not as marked as those reported for HLA-I. Nevertheless, *HLA-DRB1*15:02 and HLA-DRB1*13:01* have been associated with delayed HIV disease progression [17–19].

We reported that a high-affinity $CD4^+$ T cell response directed against the most immunodominant HIV-1 capsid epitope (Gag293) was associated with HIV-1 control [10, 15]. Across HIV controllers with different *HLA* genetic backgrounds, these $CD4^+$ T cells expressed TCRs exhibiting biased $TRAV24\text{-}TRBV2^+$ gene usage [10]. These public TCRs were highly cross-restricted, with one TCR recognizing up to five distinct HLA-DR allomorphs (HLA-

DRB1*01:01, HLA-DRB1*07:01, HLA-DRB1*11:01, HLA-DRB1*15:02, and HLA-DRB5*01:01, abbreviated to DR1, DR7, DR11, DR15, and DRB5, respectively) presenting the same Gag293 epitope. Here, we establish the mechanistic basis underpinning this broad cross-restriction and show that these public TCRs have cytotoxic capacity and kill HIV-infected cells.

RESULTS

High-affinity TCRs bind to multiple HLA-DR–Gag293 complexes

HIV controller $CD4^+$ T cells specific for the Gag293 epitope show a biased TRAV24-$TRBV2^+$ TCR repertoire, with clonotypes cross-restricted by numerous HLA-DR molecules. Whereas the HLA-DR α chain is identical, the β chains are polymorphic (**FIG**. **S1**). We set out to understand how these public TCRs could exhibit such extensive cross-restriction. We previously characterized three TRAV24-$TRBV2^+$ TCRs (F24, F25, and F5) isolated from HIV controllers, which share the same CDR3α loop but different CDR3β loops [10]. F24, F25, and F5 TCRs were cross-restricted by five, four, and two HLA-II molecules, respectively [10]. To further understand the extent of this HLA cross-restriction, we refolded the three TCRs and measured their affinity for HLA-DR15–Gag293 complex using surface plasmon resonance (SPR) [**TABLE 1** and **FIG**. **S2** [10]].

The F24 TCR bound HLA-DR molecules with greater affinity than the F25 and F5 TCRs (**TABLE 1**). The F24 TCR bound HLA-DR11 with the highest affinity observed for human CD4+ TCRs [equilibrium dissociation constant (Kdeq) ≈ 1 μM] (*20*), followed by HLA-DRB5, HLA-DR15, and HLA-DR1. Similar hierarchies were observed for the F25 and F5 TCRs (**TABLE 1**), suggesting that the CDR3β loops are modulating the affinity but not the HLA-DR hierarchy preference. The affinity hierarchy followed that of cross-restriction, suggesting that stronger binding interactions promoted recognition of the Gag293 peptide in multiple HLA contexts.

Public TCRs promote efficient mature immunological synapses

Next, we evaluated the capacity of the public TCRs to form immunological synapses with different HLA-DR molecules. We used a flow cytometry–based approach to quantify conjugate formation between TCR-expressing carboxyfluorescein diacetate succinimidyl ester (CFSE)–labelled J76 T cells and Gag293-pulsed antigen-presenting cells (APCs) (**FIG**. **S3, A and B**) (21). The frequency of conjugates was evaluated by counting the percentage of double positive CFSE+–HLA-DR+ events (**FIG**. **S3B**). Quantification of conjugate formation revealed a clear hierarchy (F24 > F25 > F5), with a similar trend observed when HLA-DR1, HLA-DR11, and HLA-DR15/DRB5 were the restricting molecules, whereas essentially no conjugates were detected with HLA-DR7 APCs (**FIG**. **1A**). The functional hierarchy observed for conjugate formation correlated well to the binding affinities of the three TCRs toward different HLA-DR molecules ($r = -0.86$, $P = 0.003$; **FIG**. **1B**), indicating that intrinsic TCR affinity is a major determinant of T cell–APC interactions.

We next compared qualitative features of mature immunological synapse (mIS) formation in the cocultures using imaging flow cytometry to examine CD3-TCR relocalization and actin rearrangements (**FIG. 1, C and D**) [22, 23]. mIS formation between J76-F24 and HLA-DR11–expressing B-EBV (Epstein-Barr virus-transformed B cells) pulsed with Gag293 was observed, whereas mere cell juxtaposition was seen in the absence of the Gag293 peptide (**FIG**. **1C**). To quantify the mIS parameters, we restricted the analysis to CD3+ HLA-DRhi doublets (**FIG**. **S3C**). We then measured the CD3 and F-actin intensities in the synapse area ("IS mask") and in the total T cell area ("T cell mask") (**FIG**. **S3D**). Conjugates with a CD3 intensity ratio of >1.1 were considered as forming a mIS. Cocultures of J76-F24 cells with HLA-DR11 APC exhibited a significantly higher proportion of mIS compared with cocultures with J76-F25 ($P = 0.008$) and J76-F5 ($P = 0.02$) cells (**FIG**. **1D**). In addition, the efficiency of actin relocalization at the mIS followed the hierarchy of TCR affinities (**FIG**. **1E**). This suggests that high-affinity TCRs confer an increased capacity to form mIS, which could lead to superior effector functions.

Public TCRs confer cytotoxic potential to $CD4^+$ and $CD8^+$ T cells

We next examined whether the expression of the three public TCRs led to the acquisition of a cytotoxic phenotype in vitro. We expressed the F24, F25, and F5 TCRs in primary T cells obtained from HLA-$DR1^+$ healthy individuals (**FIG**. S4) and stimulated these cells with Gag293-loaded autologous monocyte-derived dendritic cells (DCs) using the expression of CD107a LAMP1 and granzyme B (GrB) as indicators of cytotoxic differentiation. After Gag293 stimulation, the fraction of $CD107a^+$/GrB^+ $CD4^+$ T cells showed that a significantly higher proportion of F24-transduced $CD4^+$ T cells expressed both cytotoxic markers, followed by F25-transduced cells and then by F5-transduced cells (**FIG. 2, A and E**). These observations also extended to perforin expression, because

CD107a$^+$/perforin$^+$ cells were also enriched in Gag293-stimulated CD4$^+$ T cells expressing F24 compared with F25 and F5 TCRs (**FIG. 2, B and F**).

HLA-II–restricted TCRs can function in CD8$^+$ T cells [24], which could be advantageous in TCR transfer applications. F24-transduced primary CD8$^+$ T cells responded to Gag293 stimulation, as indicated by an increased proportion of CD107a$^+$/GrB$^+$ (**FIG. 2, C and G**) and CD107a$^+$/perforin$^+$cells (**FIG. 2, D and H**). However, in the context of CD8$^+$ T cells, responses of F25 and F5 were minimal possibly due to stronger co-receptor dependency (**FIG. 2, G and H**). These findings show that only the high-affinity F24 TCR could confer a cytotoxic phenotype in both CD4$^+$ and CD8$^+$ T cells.

Public TCRs efficiently suppress HIV replication

We next tested whether cytolytic differentiation conferred by the public TCRs could translate into direct cytotoxic effector function. We established a coculture system consisting of HIV-infected monocyte-derived DCs and TCR-transduced primary CD4$^+$ T cells (**FIG. 3, A and B**, and **FIG**. **S5A**). CD4+ T cells transduced with the F24, F25, and F5 TCRs eliminated HIV-infected DCs in the context of multiple HLA-DR–restricting molecules in an effector to target (E:T) ratio–dependent manner (**FIG. 3, C to E**).

The viral suppression mediated by CD4$^+$ T cells was highly efficient, being detected at a low E:T ratio of 0.5:1 across all HLA-DR molecules tested. Functional differences between the three TCRs were observed for HLA-DR1 (**FIG**. **3C**), and a similar hierarchical trend (F24 ≈ F25 > F5) was visible in cocultures from HLA-DR15/DRB5+ donors (**FIG**. **3E**). In cocultures from HLA-DR11$^+$ donors, the magnitude of viral suppression was comparable among the three TCRs at all E:T ratios tested (**FIG**. **3D**). Thus, HIV controller–derived TCR transfer was sufficient to confer efficient HIV-suppressive capacities to heterologous CD4+ T cells across multiple HLA-DR restrictions. Viral suppression correlated with TCR affinity ($r = -0.69$, $P = 0.039$; **FIG**. **3I**) and with conjugate formation ($r = 0.70$, $P = 0.036$; **FIG**. **3J**), suggesting that stable APC/CD4+ T cell interactions are prerequisite for efficient cytotoxic function.

We next investigated whether the three TCRs mediated clearance of HIV-infected DCs when transferred to CD8$^+$ T cells (**FIG**. **S5B**). F24-, F25-, and F5-transduced CD8$^+$ T cells all exerted viral suppression at equivalent levels in autologous HLA-DR11–expressing DCs (**FIG**. **3G**). In contrast, F24 was the sole TCR that can efficiently inhibit HIV infection in DCs expressing HLA-DR1 (**FIG**. **3F**) or HLA-DR15/DRB5 (**FIG**. **3H**). HIV-suppressive capacity correlated with TCR affinity ($r = 0.72$, $P = 0.03$; **FIG**. **3K**). However, the slope of the correlation was steeper for CD8$^+$ than CD4$^+$ T cells ($s = -35.26$ versus $s = -9.25$, respectively), suggesting that affinity requirements were more marked in the absence of co-receptor. Granzyme/CD107a induction correlated with viral suppression ($r = 0.79$, $P = 0.002$; **FIG**. **S6**), suggesting direct lysis of HIV-infected targets (**FIG**. **S7**). These findings highlighted the requirement for high-affinity TCR interactions to confer cytotoxicity against HIV-infected target cells.

Public TCRs recognize a minimal Gag293 core epitope

The Gag293 epitope is a 20-mer-long peptide located in the most conserved region of HIV-1 capsid. Because the Gag293 peptide contains four aromatic residues (anchor residues), we determined the minimal core epitope recognized by these public TCRs. We measured CD69 up-regulation in J76-F24, J76-F25, and J76-F5 cell lines in response to truncated versions of the Gag293 peptide (RE14, RQ13, or RS12; **FIG**. **4A** and **TABLE S1**). With HLA-DR11+ APCs, CD69 induction in J76-F24 cells was similar for the RE14, RQ13, and Gag293 peptides, but suboptimal for the 12-mer RS12 (**FIG**. **4A**). The three TCR cell lines responded similarly to high doses of the Gag293 and RQ13 peptides presented by HLA-DR11 and HLA-DRB5 APCs (**FIG. 4, B and C)**. However, with HLA-DR1, Gag293 was more efficiently recognized than RQ13 (**FIG**. **4D**). Our findings indicate that the RQ13 peptide (299RFYKTLRAEQASQ311) represents the minimal core region of the Gag293 epitope recognized by the public TCRs when bound to the HLA-DR1, HLA-DR11, and HLA-DRB5 molecules (**FIG**. **4**).

HLA-DR polymorphisms do not affect Gag293 presentation

Next, we determined the binary structures of the HLA-DR11 molecule presenting Gag293 and the RQ13 peptides, and the structures of HLA-DR1 and HLA-DR15 molecules in complex with the RQ13 peptide (**TABLE S2** and **FIG**. **S8**). The Gag293 and RQ13 peptides adopted the same register when binding to HLA-DR11, and their structures overlaid closely [root mean square deviation (RMSD) of the peptide, 0.18 Å]. Tyr^{301} (termed P1-Tyr) bound into the P1 pocket for both epitopes (**FIG. 4, E and F**), consistent with the RQ13 peptide representing the minimal epitope of Gag293 (**FIG. 4, A to D**).

Despite the large number of polymorphic residues across the HLA β chains (**FIG. S1**), the peptide bound in a similar conformation in all three peptide–HLA-II (pHLA-II) complexes (**FIG**. 4, F to H, and **FIG**. **S9A**). However, differences in the conformation of the HLA β chain were observed that were attributable to the polymorphisms between these HLA-DR molecules (**FIG**. **S9**). These polymorphisms result in reduced contacts between the peptide and the HLA β helix, thereby causing an opening of the hinge region of the HLA-DR15 β-chain helix (residues 63 to 73), with an RMSD of 0.7 Å compared with HLA-DR11 (**FIG**. **4I**). The HLA-DR1–RQ13 complex exhibits a larger opening of the hinge region with an RMSD of 1.6 Å, which is attributable to the polymorphic residue $Leu^{67\beta}$ and polymorphisms at the base of the cleft, namely, $Phe^{13\beta}$ and $Leu^{26\beta}$ ($Ser^{13\beta}$ and $Phe^{26\beta}$ in HLA-DR11) (**FIG**. **S9, E and F**), which has a combined effect of pushing the β helix away to avoid steric clashes with the peptide (**FIG**. **4J**). Accordingly, although the conformation of the RQ13 peptide remains similar, polymorphisms between the HLA-DR molecules alter the HLA-DR β-chain substructure itself.

The TCR β chain dominates interactions with HLA-DR11

We determined the structure of the F24 TCR–HLA-DR11–RQ13 complex (**TABLE S3**). The F24 TCR was positioned above the N-terminal region of the peptide (**FIG. 5**), adopting a docking angle of 64° across the antigen-binding cleft with a total buried surface area (BSA) upon complexation of 1830 $Å^2$, values that fall within the range observed for TCR–pMHC-II (peptide–major histocompatibility complex class II) complexes [20]. The peptide made an unusually high contribution to the interface, amounting to 45% of the pHLA BSA, which is the highest value observed for any TCR–pMHC-II complex described so far [20].

The $TRBV2^+$ β chain contributed 60% of the TCR BSA to the interface, where the CDR3β and CDR2β loops were the principal contributors to this interaction, with 34 and 14% BSA, respectively (**FIG. 5A)**. The CDR2β loop sat above the HLA-DR α chain, with Tyr57β wedged against the peptide, and made a series of interactions with HLA residues Ala64α, Val65α, and Ala68α (**FIG. 6A** and **TABLE S4**). This interaction was extended by neighboring contacts from the framework TCR β chain, with Ser66β and Glu67β hydrogen bonding to Gln57α from the HLA-DR α chain (**FIG. 6A**). The TCR β chain was characterized by predominant usage of the TRBJ2-1 and TRBD2 gene segments within the CDR3β loop [10]. This loop contacted the hinge of the HLA-DR11 β helix, where Leu109β and Met113β positioned between the P7-Glu residue and the HLA-DR11 β helix (**FIG. 6B**), whereas Arg108β and Asp114β contacted Tyr60β and Asp66β from HLA-DR11, respectively. In addition, Leu109β and Ala110β bridged across the HLA-DR11 cleft and contacted residues from both HLA α and β chains (**FIG. 6B** and **TABLE S4**). Together, the large footprint of the F24 TCR β chain provides a molecular basis for biased TCR β-chain usage.

Within the $TRAV24^+$ TCR α chain, the CDR1α loop (23% BSA) was the main contributor to the interaction (mostly via contacts with the peptide), followed by the CDR3α loop (12% BSA) (**FIG**. **5A**). Here, $Asn^{29\alpha}$ from the CDR1α loop hydrogen-bonded to $Glu^{55\alpha}$ from HLA-DR11, which abutted by the conserved TRAJ17-encoded $^{108}AAG^{110}$ motif of the CDR3α loop (**FIG**. **6C**). Thus, there was a limited role of the TCR α chain in the interaction with HLA-DR11.

The public TCR extensively contacts the RQ13 epitope

Of the 140 contacts made by the F24 TCR to the HLA-DR11–RQ13 complex, 63% were directed toward the peptide, indicating peptide-centric recognition (**FIG**. **5A** and **TABLE S4**). The contacts were evenly distributed between the TCR α and β chains with almost all CDR loops involved in peptide contact, with the following contribution hierarchy: CDR1α (55%) > CDR3β (25%) > CDR1β (10%) > CDR2β = CDR3α (5%) (**FIG**. **5A**). The unusually high contribution of the germline-encoded CDR1α loop to the TCR-peptide interactions provided a molecular basis for the TRAV24 bias. The CDR1α loop contacted P-1-Phe, P2-Lys, and P3-Thr (**FIG**. **6D**). Here, $Asn^{29\alpha}$ packed against P-1-Phe, whereas $Tyr^{31\alpha}$ lodged between the P2-Lys and P5-Arg, directly interacting with the P2-Lys and the main chain of P3-Thr. P5-Arg was "boxed in" by two CDR3 loops, and by $Tyr^{31\alpha}$ and $Tyr^{31\beta}$ from both CDR1 loops (**FIG. 6, D and E**). Residues within the CDR3 loops interacting with the P5-Arg involved $^{109}AGN^{111}$ from the TRAJ17 region and $^{110}AG^{111}$ region from the TRBD2 segment (**FIG**. **6E** and **TABLE S4**). In addition, the CDR3β loop wrapped itself around P7-Glu, forming a salt bridge with $Arg^{108\beta}$, whereas the P8-Gln was contacted by the CDR1β and CDR2β loops via $Leu^{30\beta}$ and $Tyr^{57\beta}$, respectively (**FIG. 6F** and **TABLE S4**). Together, the germline-encoded TCR segments contacted the entire length of the core peptide, explaining the highly biased nature of the Gag293-specific TCR repertoire.

Although the F24 TCR differs from the F5 TCR by a single residue in the CDR3β loop ($Arg^{108\beta}$→$Gly^{108\beta}$), there is a 12-fold difference in affinity for the HLA-DR11–RQ13 complex between these two TCRs (**TABLE 1**). The structure of the F24 and F5 TCRs in complex with HLA-DR11–RQ13 (**TABLE S3** and **FIG**. **S10**) revealed that a

lack of contact between Gly$^{108\beta}$ and P7-Glu underpins the large affinity reduction of the F5 TCR for HLA-DR11–RQ13 (**FIGs. 1 and 3** and **TABLE 1)**. Thus, a single CDR3β residue substitution can markedly decrease the extent of T cell cross-restriction by decreasing the TCR affinity.

HLA-DR cross-restriction is underpinned by an induced-fit mechanism

The F24 TCR contacted 11 residues on HLA-DR11: 6 from the HLA-DR α chain and 5 from the HLA-DR β chain (**TABLE S4**). Of these contact points, two residues (Gln$^{64\beta}$ and Asp$^{66\beta}$) within the β chain are conserved across the five cross-restricted HLA-DR molecules, whereas the other three positions (60β, 67β, and 73β) are polymorphic (**FIG**. **S1**). Accordingly, it was unclear whether the F24 TCR would adopt different docking modes on the other HLA-DR molecules.

We determined the structures of the F24 TCR in complex with HLA-DR15–RQ13 and HLA-DR1–RQ13 (**FIGs. 5 to 7** and **TABLE** S3). Relative to the F24 TCR–HLA-DR11–RQ13 ternary complex, the F24 TCR bound HLA-DR15–RQ13 and HLA-DR1–RQ13 similarly (**FIG. 5, B and C**, and **TABLES S5 and S6**). Accordingly, TCR cross-restriction was not attributable to diverse TCR docking modes across the distinct HLA-DR allomorphs.

To understand how the F24 TCR might accommodate the HLA-DR conformational differences, we determined the structure of the unliganded F24 TCR (**TABLE S7**). The CDR3β loop changed conformation (**FIG**. **S11**) to avoid steric clashes with the hinge of the HLA-DR11 β-chain helix. Although there was no structural alteration in the HLA-DR11 molecule upon F24 TCR binding (**FIG**. **7A**), the antigen-binding clefts of HLA-DR15 and HLA-DR1 were molded upon F24 TCR binding (**FIG. 7, B and C**). Namely, the hinge of the HLA β chain of both HLA-DR1 and HLA-DR15 was shifted by 1 and 0.7 Å (residues 63 to 73β), respectively, upon TCR binding (**FIG. 7, B and C**). This movement resulted in a closing of the HLA-DR1 and HLA-DR15 antigen-binding clefts, resulting in the two HLA molecules becoming more similar to the HLA-DR11 structure upon TCR engagement. Accordingly, structural rearrangement occurred upon TCR binding that modulated the affinity toward the different HLA-DR molecules. The HLA-DR β-chain polymorphism could be accommodated, thereby favoring the broad cross-restriction observed by the public TCR.

Public TCR recognition is driven by the HIV peptide

It was unclear whether the conserved features of the HLA-DR residues or the RQ13 peptide were responsible for the conserved F24 TCR docking. To clarify this, we performed mutagenesis of the HLA-DR11 residues contacted by the F24 TCR, and determined their energetic contributions by SPR (**FIG. 7, D to F; FIG**. **S12;** and **TABLE S8**). We produced nine single-site HLA-DR11 mutants, targeting the conserved and the polymorphic HLA-DR residues (**TABLE S4**), the impact of which was tested against the F24, F25, and F5 TCRs. The mutants exhibited a similar pattern of binding across all three TCRs, indicating a common docking modality (**FIG. 7, D to F**, and **TABLE S8**). Strikingly, the TCR affinities were not decreased by any of the HLA-DR11 β-chain mutants.

The three TCRs were not affected by mutations at Ala$^{64\alpha}$, Val$^{65\alpha}$, and Gln$^{57\alpha}$, whereas the Ala$^{68\alpha}$Leu and Glu$^{55\alpha}$Ala mutations decreased the affinity of the interaction by more than fivefold (**TABLE S8**). The CDR2β Tyr$^{57\beta}$ contacted the HLA-DR11 Ala$^{68\alpha}$, and the Ala→Leu mutation would be sterically disfavored (**FIG**. **6A**). Glu$^{55\alpha}$ is hydrogen-bonded to Asn$^{29\alpha}$ from the CDR1α loop and formed van der Waals contacts with the CDR3α loop of the F24 TCR (**FIG**. 6C). In summary, from the HLA molecule itself, only residues shared across all HLA-DR (Glu$^{55\alpha}$ and Ala$^{68\alpha}$) were energetically important for public TCR recognition.

We next performed alanine scanning mutagenesis of the RQ13 peptide by mutating five solvent-exposed residues contacted by the F24 TCR (**FIG**. 4). P2, P5, and P7 mutants abrogated F24 responses to HLA-DR11^{+} APCs (**FIGs. 4B and 7D**), whereas all five positions were crucial for HLA-DR1^{+} APCs (**FIGs. 4B and 7H**). Furthermore, all five mutations markedly reduced F5 and F25 responses to HLA-DR11 APCs (**FIGs. 4B and 7, E and F**). In the context of HLA-DRB5^{+} APCs, all five residues abrogated the F24 TCR response (**FIGs. 4C and 7G**). Thus, alongside two residues within the HLA-DR α chain, the RQ13 determinants represent the critical energetic hotspot underpinning public TCR recognition across multiple HLA-DR allomorphs.

Public TCR usage is optimized to engage the Gag293 peptide

Next, we undertook an alanine scanning mutagenesis approach on the F24 TCR residues that contacted the HLA-DR11–RQ13 complex (**TABLE S9**), and tested, via SPR, each F24 TCR mutant against the HLA-DR11, HLA-DR1, HLA-DR15, and HLA-DRB5 molecules presenting the RQ13 peptide. Six F24 TCR α-chain mutants and eight F24

TCR β-chain mutants were generated (**TABLE S9**). The $Thr^{22\alpha}Ala$ mutant, which was not involved in the interaction, was used as control and did not affect the affinity of the F24 TCR (**TABLE S9**).

The F24 TCR mutations affected recognition of the four HLA-DR–RQ13 complexes similarly. Here, only two TCR mutants ($Leu^{58\alpha}$ and $Ser^{66\beta}$), both of which contacted the HLA molecule solely, did not decrease the affinity of the F24 TCR for any of the HLA-DR molecules tested. In contrast, mutations of the other F24 TCR residues decreased the affinity of the interaction by more than ninefold for all the HLA-DR molecules tested (**TABLE S9**). Here, five F24 TCR residues ($Tyr^{31\alpha}$, $Lys^{107\alpha}$, $Asn^{111\alpha}$, $Leu^{30\beta}$, and $Tyr^{31\beta}$) solely contacted the HIV epitope, whereas six residues co-recognized the RQ13 peptide and the HLA molecule. However, on the basis of the HLA mutagenesis (above), only two residues ($Asn^{29\alpha}$ and $Tyr^{57\beta}$) were considered to make energetically important contributions toward contacting the HLA molecule itself, whereas the impact of the remaining four mutants ($Glu^{67\beta}$, $Arg^{108\beta}$, $Leu^{109\beta}$, and $Met^{113\beta}$) was more attributable to peptide-mediated contacts.

These energetically critical residues of the F24 TCR formed a stretch that travelled across the length of the RQ13 peptide (**FIG**. 7I). Thus, public TRAV24-TRBV2$^+$ TCR usage and extensive HLA-II cross-restriction are, to a large extent, attributable to peptide-centric recognition.

DISCUSSION

A key factor in the public TCR recognition of the HLA-DR–Gag293 complexes is engagement of the HIV epitope itself, thereby providing a basis for the extensive HLA-DR cross-restriction. Furthermore, the high-affinity public TCRs conferred anti-HIV cytotoxic activity to heterologous CD4$^+$ and CD8$^+$ T cells across multiple HLA-DR molecules. Because the TCR affinity directly correlated with the cytotoxic capacity of the TCR-transduced T cells, our results emphasize the importance of TCR structural determinants in defining a protective outcome.

Given the predominance of high-affinity Gag293-specific TCRs in HIV controllers [10, 15], our findings suggest that CD4$^+$ T cells expressing such TCRs directly contribute to HIV control. The emergence of cytotoxic CD4$^+$ T cells in acute HIV infection is associated with a more efficient control of HIV replication in the post-acute stage [13], suggesting that CD4-dependent cytotoxic activity may act very early. The broad HLA-DR cross-restriction is likely to confer a protective advantage in HIV infection because it increases the chance of epitope detection in a single individual expressing multiple restricting *HLA-DR* alleles. Broad HLA restriction also explains the high frequency of public TCR sharing among genetically diverse HIV controllers. The high frequency of high-affinity Gag-specific TCRs in HIV controller CD4$^+$ T cells may translate to a more efficient curtailing of HIV dissemination at an early stage, accounting for the very low viral reservoir characteristic of controlled HIV infection [25]. Our findings support a contribution of CD4$^+$ cytotoxic T cells, in addition to cytotoxic CD8$^+$ T cells [3, 5, 7] and natural killer cells [26, 27], to HIV control. Thus, the cooperation of multiple arms of the cellular response may be required to efficiently contain the population of HIV-infected target cells.

TCR affinity is known to condition the capacity of CD4$^+$ T cells to proliferate, survive as long-term memory cells, and show polyfunctional cytokine secretion [4, 10], which define a series of properties characteristic of HIV controller CD4$^+$ T cells [14, 17, 28]. We show here that TCR affinity is also a key determinant of CD4$^+$ T cell cytotoxic function, which has major implications for understanding the basis of HIV control. Recent findings suggest that cellular factors independent of TCR affinity may also contribute to the efficient cytolytic capacity of HIV controller CD8$^+$ T cells [29]. A limitation of our study is that we did not assess TCR-independent factors, such as the expression of costimulatory receptors. Nevertheless, we have shown that transfer of a high-affinity TCR was sufficient to confer efficient lysis of HIV-infected target cells, which may be harnessed for immunotherapeutic purposes.

The ability of the public TCRs to recognize multiple HLA-DR allomorphs is noteworthy. The extensive HLA cross-restriction was attributable to the promiscuous Gag293 peptide binding of HLA-DR molecules and peptide-centric nature of the interaction, where multiple residues along the entire length of the RQ13 peptide and two invariant HLA-DRα residues were essential for the interaction. Moreover, whereas the conformation of the HIV epitope was conserved upon TCR engagement and across the HLA-DR molecules, the conformation of some of the HLA molecules was pliable upon TCR engagement, indicating that an induced-fit molecular mimicry mechanism underpinned the observed hierarchy of TCR cross-restriction.

We provide detailed molecular insight into $CD4^+$ T cell–mediated recognition of HIV-1 in controller individuals, which has broad therapeutic implications. In particular, HLA cross-restricted public TCRs could represent valuable tools for immunotherapeutic applications aimed at a functional HIV cure, because TCR transfer could be considered in patients with diverse genetic backgrounds. In addition, the capacity of the high-affinity public TCRs to confer cytotoxic capacity to both $CD4^+$ and $CD8^+$ T cells would be an asset, by harnessing both arms of the T cell response for the elimination of HIV-1–infected target cells.

MATERIALS AND METHODS

Study design

The aim of the study was to determine the basis of TCR HLA cross-restriction, HIV peptide recognition by $CD4^+$ T cells, and HIV inhibition and cytotoxic capability of HIV-specific $CD4^+$ T cells. To enable this, we undertook experiments centered on cellular immunology, imaging flow cytometry, protein chemistry, SPR binding studies, and protein x-ray crystallography. The number of independent experiments is outlined in the figure legends, where appropriate.

REFERENCES

1. International AIDS Society Scientific Working Group on HIV Cure, S.G. Deeks, B Autran, B. Berkhout, M. Benkirane, S. Cairns, N. Chomont, T.W. Chun, M. Churchill, M. Di Mascio, C. Katlama, A. Lafeuillade, A. Landay, M. Lederman, S.R. Lewin, F. Maldarelli, D. Margolis, M. Markowitz, J. Martinez-Picado, J.I. Mullins, J. Mellors, S. Moreno, U. O'Doherty, S. Palmer, M.C. Penicaud, M. Peterlin, G. Poli, J.P. Routy, C. Rouzioux, G. Silvestri, M. Stevenson, A. Telenti, C.V an Lint, E. Verdin, A. Woolfrey, J. Zaia, F. Barré-Sinoussi. **Towards an HIV cure: A global scientific strategy.** Nat. Rev. Immunol. 12,607–614(2012).

2. S. Grabar, H. Selinger-Leneman, S. Abgrall, G. Pialoux, L. Weiss, D. Costagliola. **Prevalence and comparative characteristics of long-term nonprogressors and HIV controller patients in the French Hospital Database on HIV.** AIDS **23**, 1163–1169 (2009)

3. J.R. Almeida, D.A. Price, L. Papagno, Z.A. Arkoub, D. Sauce, E. Bornstein, T.E. Asher, A. Samri, A. Schnuriger, I. Theodorou, D. Costagliola, C. Rouzioux, H. Agut, A.G. Marcelin, D. Douek, B. Autran, V. Appay. **Superior control of HIV-1 replication by CD8$^+$ T cells is reflected by their avidity, polyfunctionality, and clonal turnover**. J. Exp. Med. **204**, 2473–2485 (2007)

4. J. R. Almeida, D. Sauce, D. A. Price, L. Papagno, S. Y. Shin, A. Moris, M. Larsen, G. Pancino, D. C. Douek, B. Autran, A. Sáez-Cirión, V. Appay**. Antigen sensitivity is a major determinant of CD8$^+$ T-cell polyfunctionality and HIV-suppressive activity**. Blood **113**, 6351–6360 (2009).

5. K. Ladell, M. Hashimoto, M.C. Iglesias,.P.G. Wilmann, J.E. McLaren, S. Gras, T. Chikata, N. Kuse, S. Fastenackels, E. Gostick, J. S. Bridgeman, V. Venturi, Z. A. Arkoub, H. Agut, D. J. van Bockel, J. R. Almeida, D. C. Douek, L. Meyer, A. Venet, M. Takiguchi, J. Rossjohn, D. A. Price, V. Appay. **A molecular basis for the control of preimmune escape variants by HIV-specific CD8$^+$ T cells**. Immunity **38**, 425–436 (2013).

6. Košmrlj, E.L. Read, Y. Qi, T.M. Allen, M. Altfeld, S. Deeks, F. Pereyra, M. Carrington, B. D. Walker, A. K. Chakraborty. **Effects of thymic selection of the T-cell repertoire on HLA class I-associated control of HIV infection.** Nature **465**, 350–354 (2010)

7. J. R. Almeida, D. Sauce, D. A. Price, L. Papagno, S. Y. Shin, A. Moris, M. Larsen, G. Pancino, D. C. Douek, B. Autran, A. Sáez-Cirión, V. Appay**.. Antigen sensitivity is a major determinant of CD8$^+$ T-cell polyfunctionality and HIV-suppressive activity**. Blood **113**, 6351–6360 (2009).

8. M.C. Iglesias, J.R. Almeida, S. Fastenackels, D.J. vanBockel, M. Hashimoto, V. Venturi, E. Gostick, A.Urrutia , L. Wooldridge, M. Clement, S. Gras, P.G. Wilmann,B. Autran, A. Moris, J. Rossjohn, M.P. Davenport,.M. T akiguchi,
C. Brander, D. C. Douek, A. D. Kelleher, D. A. Price, V. Appay. **Escape from highly effective public CD8$^+$ T-cell clonotypes by HIV.** Blood **118**, 2138–2149 (2011).

9. A. Sáez.Cirión, C. Lacabaratz, O. Lambotte, P. Vermisse, A. Urrutia, F. Boufassa, F. Barré-Sinoussi, J.-F.Delfraissy, M. Sinet, G. Pancino, A. Venet. **ANRS EP36 HIV CONTROLLERS study group. HIV controllers exhibit potent CD8 T cell capacity to suppress HIV infection ex vivo and peculiar cytotoxic T lymphocyte activation phenotype**. Proc. Natl. Acad. Sci. U.S.A. **104**, 6776–6781 (2007

10. D. Benati, M. Galperin, O. Lambotte, S. Gras, A. Lim, M. Mukhopadhyay, A. Nouël, K.A. Campbell, B. Lemercier, M. Claireaux, S. Hendou, P. Lechat, P. deTruchis, F. Boufassa, J. Rossjohn, J.F. Delfraissy, F.Arenzana-Seisdedos, L. A. Chakrabarti**. Public T cell receptors confer high-avidity CD4 responses to HIV controllers.** J. Clin. Invest. **126**, 2093–2108 (2016).

11. S. Johnson, M. Eller, J.E. Teigler, S.M. Maloveste, B.T. Schultz, D..Z. Soghoian, R. Lu, A.F. Oster, A.L.Chenine, G. Alter, U. Dittmer, M. Marovich, M.L. Robb, N.L. Michael, D. Bolton, H. Streeck. **Cooperativity of HIV-specific cytolytic CD4 T cells and CD8 T cells in control of HIV viremia**. J. Virol. 89, 7494–7505(2015).

12. J. B. Sacha, J. P. Giraldo-Vela, M. B. Buechler, M. A. Martins, N. J. Maness, C. Chung, L. T. Wallace, E. J. León, T. C. Friedrich, N. A. Wilson, A. Hiraoka, D. I. Watkins. **Gag- and Nef-specific CD4$^+$ T cells recognize and inhibit SIV replication in infected macrophages early after infection**. Proc. Natl. Acad. Sci. U.S.A. **106**,9791–9796 (2009).

13. D. Z. Soghoian, H. Jessen, M. Flanders, K. Sierr.Davidson, S. Cutler, T. Pertel, S. Ranasinghe, M.Lindqvist, I. Davis, K. Lane, J. Rychert, E.S. Rosenberg, A. Piechocka.Trocha, A.L. Brass, J.. Brenchley, B.D. Walker, H. Streeck. **HIV-specific cytolytic CD4 T cell responses during acute HIV infection predict disease outcome**. Sci. Transl. Med. **4**, 123ra25 (2012).

14. D. E. Kaufmann, D. G. Kavanagh, F. Pereyra, J. J. Zaunders, E. W. Mackey, T. Miura, S. Palmer, M. Brockman, A. Rathod, A. Piechocka-Trocha, B. Baker, B. Zhu, S. Le Gall,M. T. Waring, R. Ahern, K. Moss, A. D. Kelleher, J. M. Coffin, G. J. Freeman, E. S. Rosenberg, B. D. Walker. **Upregulation of CTLA-4 by HIV-specific CD4$^+$ T cells correlates with disease progression and defines a reversible immune dysfunction**. Nat. Immunol. **8**, 1246–1254 (2007).

15. B. Vingert, S. Perez-Patrigeon, P. Jeannin, O. Lambotte, F. Boufassa, F. Lemaitre, W. W. Kwok, I. Theodorou, J.-F. Delfraissy, J. Thèze, L. A. Chakrabarti, ANRS EP36 HIV Controllers Study Group. **HIV controller CD4$^+$ T cells respond to minimal amounts of Gag antigen due to high TCR avidity.** PLOS Pathog.**6**, e1000780 (2010).

16. B. Vingert, D. Benati, O. Lambotte, P. de Truchis, L. Slama, P. Jeannin, M. Galperin, S. Perez-Patrigeon, F.Boufassa, W. W. Kwok, F. Lemaître, J.-F. Delfraissy, J. Thèze, L. A. Chakrabarti**. HIV controllers maintain a population of highly efficient Th1 effector cells in contrast to patients treated in the long term**. J. Virol. **86**,10661–10674 (2012).

17. A. L. Ferre, P. W. Hunt, D. H. McConnell, M. M. Morris, J. C. Garcia, R. B. Pollard, H. F. Yee Jr, J. N. Martin,
S. G. Deeks, B. L. Shacklett**. HIV controllers with HLA-DRB1*13 and HLA-DQB1*06 alleles have strong, polyfunctional mucosal CD4$^+$ T-cell responses**. J. Virol. **84**, 11020–11029 (2010)

18. U. Malhotra, S. Holte, S. Dutta, M. M. Berrey, E. Delpit, D. M. Koelle, A. Sette, L. Corey, M.J. McElrath, **Role for HLA class II molecules in HIV-1 suppression and cellular immunity following antiretroviral treatment.** J. Clin. Invest. **107**, 505–517 (2001).

19. S. Ranasinghe, S. Cutler, I. Davis, R. Lu, D.Z. Soghoian, Y. Qi, J. Sidney, G. Kranias, M.D. Flanders, M. Lindqvist, B. Kuhl, G. Alter, S.G. Deeks, B.D. Walker, X. Gao, A. Sette, M. Carrington, H. Streeck. **Association of HLA-DRB1–restricted CD4$^+$ T cell responses with HIV immune control**. Nat. Med. **19**, 930–933 (2013).

20. J. Rossjohn, S. Gras, J. J. Miles, S. J. Turner, D. I. Godfrey, J. McCluskey. **T cell antigen receptor recognition of antigen-presenting molecules**. Annu. Rev. Immunol. **33**, 169–200 (2015).

21. M. H. M. Heemskerk, M. Hoogeboom, R.A. dePaus, M.G.D. Kester, M.A.W.G. vanderHoorn, E.Goulmy, R. Willemze, J. H. F. Falkenburg. **Redirection of antileukemic reactivity of peripheral T lymphocytes using gene transfer of minor histocompatibility antigen HA-2-specific T-cell receptor complexes expressing a conserved alpha joining region.** Blood **102**, 3530–3540 (2003).

22. M. L. Dustin, K. Choudhuri. **Signaling and polarized communication across the T cell immunological synapse.** Annu. Rev. Cell Dev. Biol. **32**, 303–325 (2016).

23. C. R. F. Monks, B. A. Freiberg, H. Kupfer, N. Sciaky, A. Kupfer. **Three-dimensional segregation of supramolecular activation clusters in T cells.** Nature **395**, 82–86 (1998).

24. S. Ranasinghe, P. A. Lamothe, D. Z. Soghoian, S. W. Kazer, M. B. Cole,A. K. Shalek, N. Yosef, R. B. Jones, F. Donaghey, C. Nwonu, P. Jani, G. M. Clayton, F. Crawford, J. White, A. Montoya, K. Power, T. M. Allen, H.Streeck, D. E. Kaufmann, L. J. Picker, J. W. Kappler, B. D. Walker. **Antiviral CD8$^+$ T cells restricted by human leukocyte antigen class II exist during natural HIV infection and exhibit clonal expansion.** Immunity **45**,917–930 (2016).

25. S. R. Lewin, C. Rouzioux. **HIV cure and eradication: How will we get from the laboratory to effective clinical trials?** AIDS **25**, 885–897 (2011).

26. V. Ramsuran, V. Naranbhai, A. Horowitz, Y. Qi, M. P. Martin, Y. Yuki, X. Gao, V. Walker-Sperling, G. Q. Del Prete, D. K. Schneider, J. D. Lifson, J. Fellay, S. G. Deeks, J. N. Martin, J. J. Goedert, S. M. Wolinsky, N. L.Michael, G. D. Kirk, S. Buchbinder, D. Haas, T. Ndung'u, P. Goulder, P. Parham, B.

D. Walker, J. M. Carlson, M.Carrington. **Elevated *HLA-A* expression impairs HIV control through inhibition of NKG2A-expressing cells.** Science **359**, 86–90 (2018).

27. M. P. Martin, V. Naranbhai, P. R. Shea, Y. Qi, V. Ramsuran, N. Vince, X. Gao, R. Thomas, Z. L. Brumme, J. M. Carlson, S. M. Wolinsky, J. J. Goedert, B. D. Walker, F. P. Segal, S. G. Deeks, D. W. Haas, S. A. Migueles, M. Connors, N. Michael, J. Fellay, E. Gostick, S. Llewellyn-Lacey, D. A. Price, B. A. Lafont, P. Pymm, P. M. Saunders, J. Widjaja, S. C. Wong, J. P. Vivian, J. Rossjohn, A. G. Brooks, M. Carrington**. Killer cell immunoglobulin–like receptor 3DL1 variation modifies HLA-B*57 protection against HIV-1**. J. Clin. Invest.**128**, 1903–1912 (2018).

28. S.-A. Younes, B. Yassine-Diab, A. R. Dumont, M. R. Boulassel, Z. Grossman, J.-P. Routy, R.-P. Sékaly. **HIV-1 viremia prevents the establishment of interleukin 2–producing HIV-specific memory CD4$^+$ T cells endowed with proliferative capacity.** J. Exp. Med. **198**, 1909–1922 (2003).

29. N. C. Flerin, H. Chen, T. D. Glover, P. A. Lamothe, J. H. Zheng, J. W. Fang, Z. M. Ndhlovu, E. W. Newell, M. M. Davis, B. D. Walker, H. Goldstein. **T-Cell receptor (TCR) clonotype-specific differences in inhibitory activity of HIV-1 cytotoxic T-cell clones is not mediated by TCR alone**. J. Virol. **91**, e02412-16 (2017).

30. E. P. Klohe, R. Watts, M. Bahl, C. Alber, W. Y. Yu, R. Anderson, J. Silver, P. K. Gregersen, R. W. Karr. Analysis of the molecular specificities of anti-class II monoclonal antibodies by using L cell transfectants expressing HLA class II molecules. J. Immunol. **141**, 2158–2164 (1988).

31. D. Nègre, P.-E. Mangeot, G. Duisit, S. Blanchard, P.-O. Vidalain, P. Leissner, A.-J. Winter, C. Rabourdin-Combe, M. Mehtali, P. Moullier, J.-L. Darlix, F.-L. Cosset. **Characterization of novel safe lentiviral vectors derived from simian immunodeficiency virus (SIVmac251) that efficiently transduce mature human dendritic cells.** Gene Ther. **7**, 1613–1623 (2000).

32. Collaborative Computational Project, Number 4. The CCP4 suite: **Programs for protein crystallography**. Acta Crystallogr. D Biol. Crystallogr. **50**, 760–763 (1994).

FIG 1

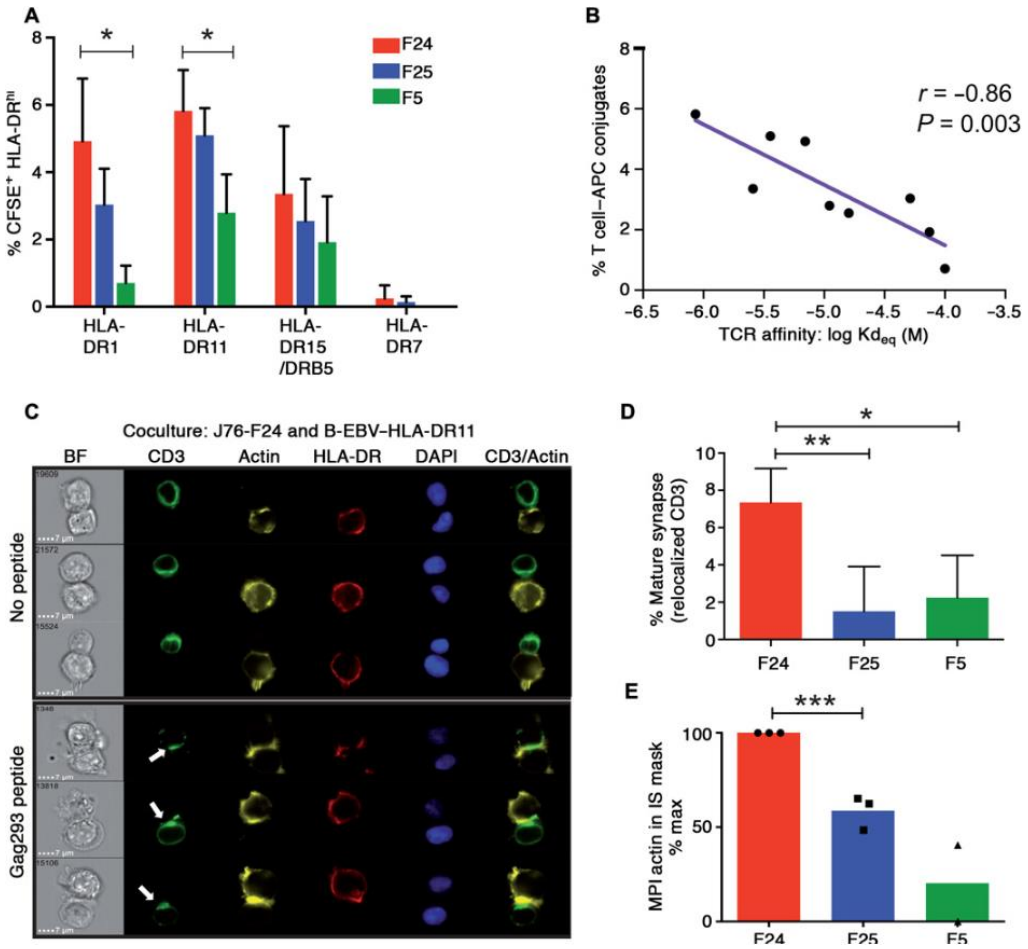

Immunological synapse formation by public TCR-transduced cells.

(**A**) Bar graphs summarizing the conjugate formation of the F24-transduced (red), F25-transduced (blue), and F5-transduced (green) J76 cells with Gag293-pulsed B-EBV cells ($n = 3$). (**B**) Correlation between TCR affinity (**TABLE** 1) and conjugate formation capacity ($n = 3$). *r*, Pearson coefficient. (**C**) Representative images obtained by imaging flow cytometry comparing mIS formation. CD3 recruitment to the T cell–APC contact site is indicated by a white arrow. DAPI, 4′,6-diamidino-2-phenylindole. (**D**) Bar graph comparing the % mIS formed between J76 cells expressing F24 (red), F25 (blue), or F5 (green), and DR11-expressing B-EBV cells, with means ± SD reported ($n = 4$ except for F5, $n = 3$). (**E**) Bars depict the actin mean pixel intensity (MPI) values represented as the percentage of the maximal response (F24 + DR11–B-EBV), with data points reported as black symbols ($n = 3$ except for F5, $n = 2$). Statistical differences are computed using unpaired Student's *t* test. Background was subtracted for all samples. *$P < 0.05$, **$P < 0.01$, ***$P < 0.005$.

FIG 2

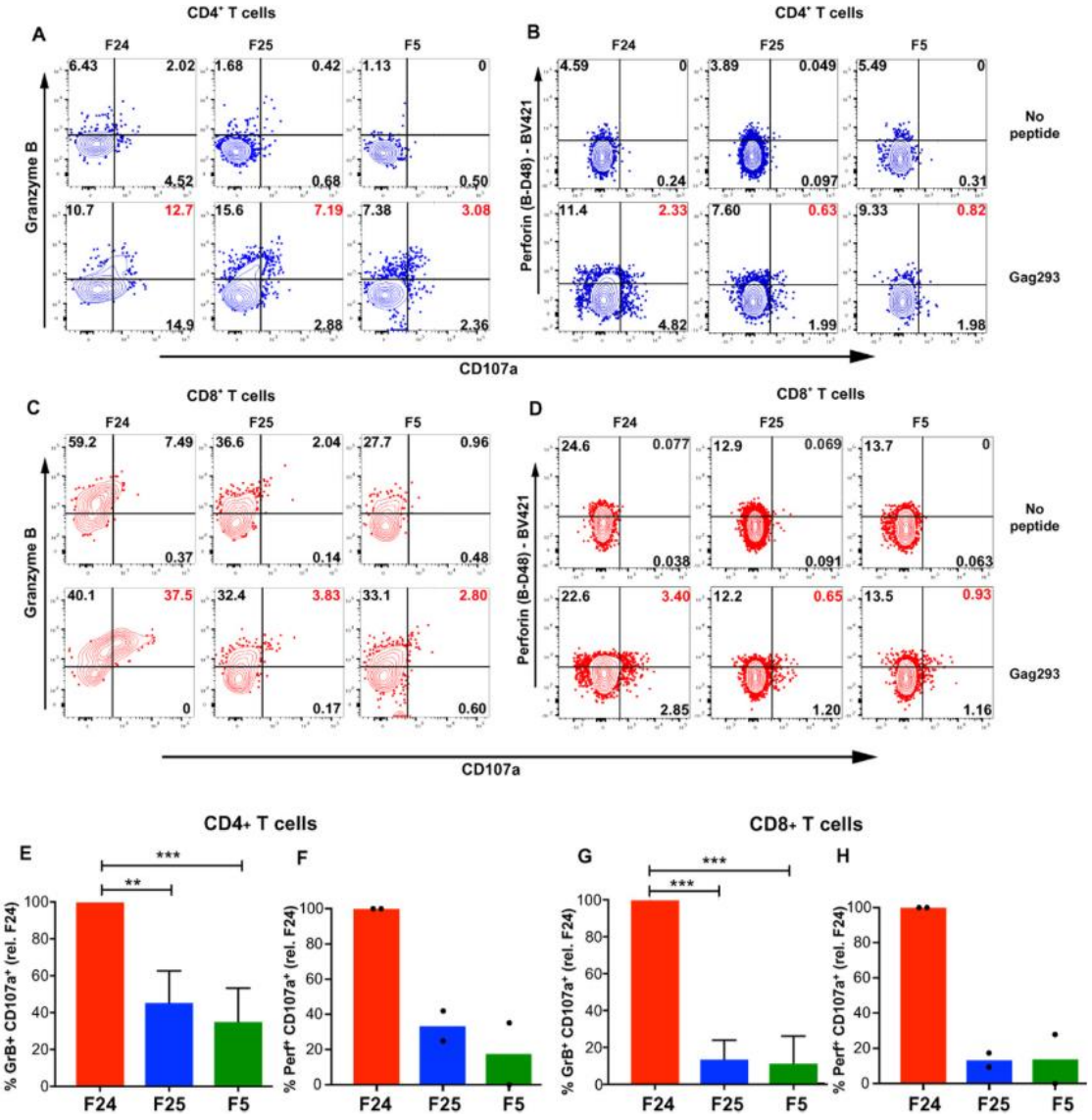

TCR-transduced T cells express cytotoxic markers upon Gag293 stimulation.

(**A** to **D**) Fluorescence-activated cell sorting plots depicting the expression of CD107a and GrB (A and C) or CD107a and perforin (B and D) by F24-transduced (left), F25-transduced (middle), or F5-transduced (right) primary $CD4^+$ T cells. The % of double positive cells is highlighted in red. (**E** to **H**) Bar graphs summarizing the proportion of cytotoxic $CD107a^+GrB^+$ (E and G) or $CD107a^+$ $perforin^+$ (F and H) $CD4^+$ T cells (E and F) or $CD8^+$ T cells (G and H) transduced with F24 (red), F25 (blue), or F5 TCR (green). Data are depicted as % of the maximal response obtained with F24-transduced T cells, with means ± SD reported for $CD107^+$ GrB^+ (n = 3) and means reported for $CD107^+$ $perforin^+$ (n = 2), with data points reported as black symbols. Statistical differences are computed using the unpaired Student's t test. Background was subtracted from all data points. $^{**}P < 0.01$, $^{***}P < 0.005$.

FIG 3

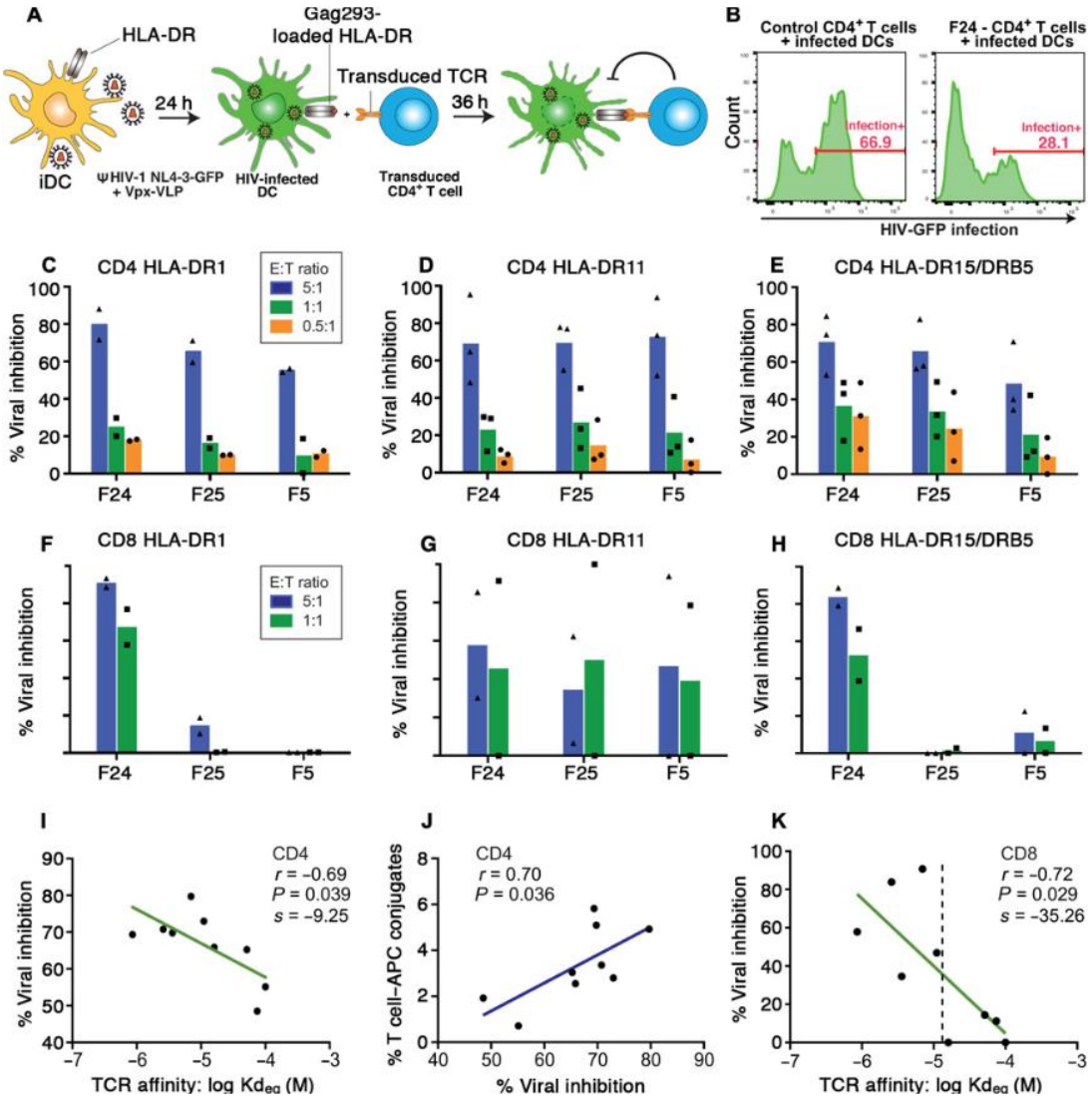

Viral suppression by TCR-transduced CD4⁺ and CD8⁺ T cells.

(**A**) Schematic representation of the experimental system. Viral inhibition was measured by the % decrease of green fluorescent protein–positive (GFP^+) infected DCs (iDC). (**B**) Representative histograms displaying the viral inhibition effect mediated by F24-transduced $CD4^+$ T cells (right) compared with nontransduced $CD4^+$ T cells (left). The % infected iDC is highlighted in red. (**C** to **E**) Viral inhibition activity of TCR-transduced $CD4^+$ T cells from healthy donors expressing HLA-DR1 (C), HLA-DR11 (D), or HLA-DR15/DRB5 (E). E:T ratios: 5:1 (blue), 1:1 (green), and 0.5:1 (orange). Bars depict the means obtained from two (C) or three (D and E) independent experiments. Background was subtracted from all data points. (**F** to **H**) Viral inhibition activity of TCR-transduced $CD8^+$ T cells from HLA-DR1 (F), HLA-DR11 (G), or HLA-DR15/DRB5 (H) healthy donors. Bars in (F) to (H) depict the means of two independent experiments. The mean % of viral inhibition obtained by TCR-transduced $CD4^+$ T cells (**I**) or $CD8^+$ T cells (**K**) coculture at a 5:1 E:T ratio is plotted in function of TCR affinities. (**J**) The mean % of viral inhibition obtained by TCR-transduced $CD4^+$ T cells is plotted in function of the mean % conjugates formed (reported in **FIG**. 1A). Data points are reported as black symbols.

FIG 4

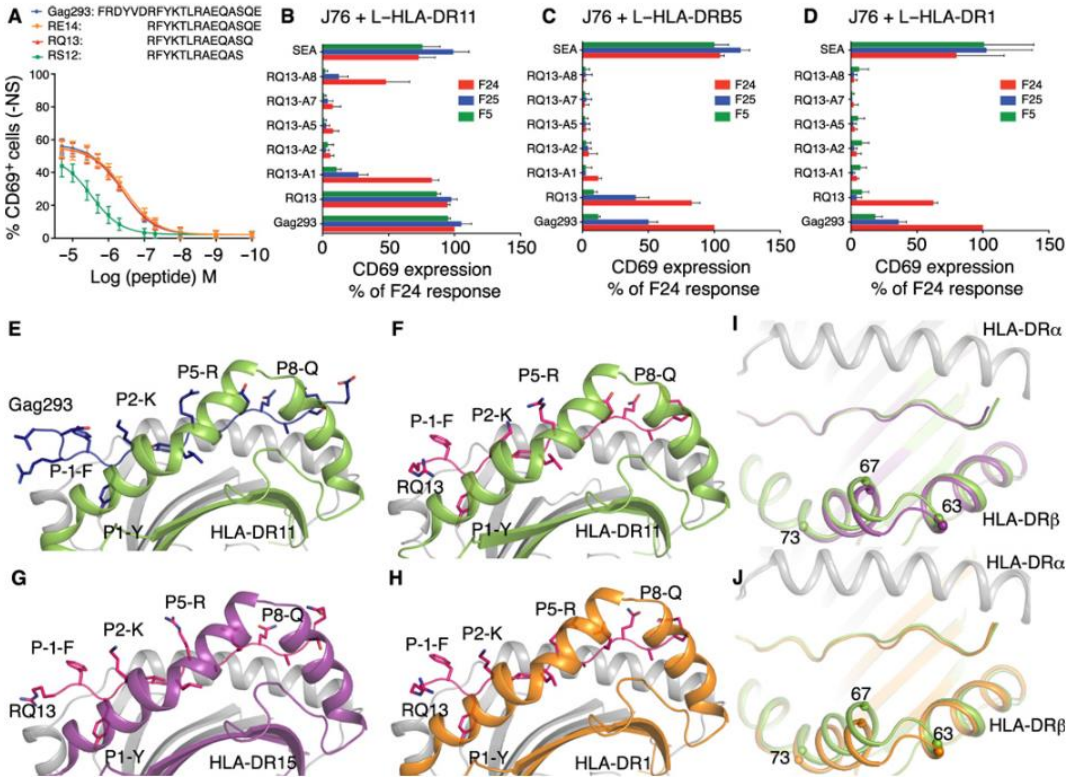

Mapping of the core Gag293 epitope and peptide presentation.

(**A**) F24-transduced J76 cells were cocultured with APC pulsed with serial dilutions of either full-length Gag293 or peptide truncations. TCR activation was measured by CD69 induction, with background subtracted from all samples. Means ± SD are reported (n = 3). (**B** to **D**) J76 cells transduced with either F24 (red), F25 (blue), or F5 (green) were cocultured with HLA-DR11–expressing (B), HLA-DRB5–expressing (C), or HLA-DR1–expressing (D) L cells in the presence of the core-epitope RQ13 or alanine mutants. Means ± SD are reported (n= 3). (**E** to **J**) Structures of the peptide-HLA complexes with the Gag293 peptide (blue stick) or the RQ13 peptide (pink stick) (F to H). The β chain of HLA-DR11 is colored green (E, F, I, and J), HLA-DR15 is purple (G and I), HLA-DR1 is orange (H and J), and the HLA-DR α chain is pale gray. Structure overlay of HLA-DR11–RQ13 (green) with HLA-DR15–RQ13 (purple) (I) and HLA-DR15–RQ13 (orange) (J), with the peptide colored similarly to the HLA-DR β chain. The HLA-DR β chain residues 63, 67, and 73 Cα atoms are shown as spheres.

FIG 5

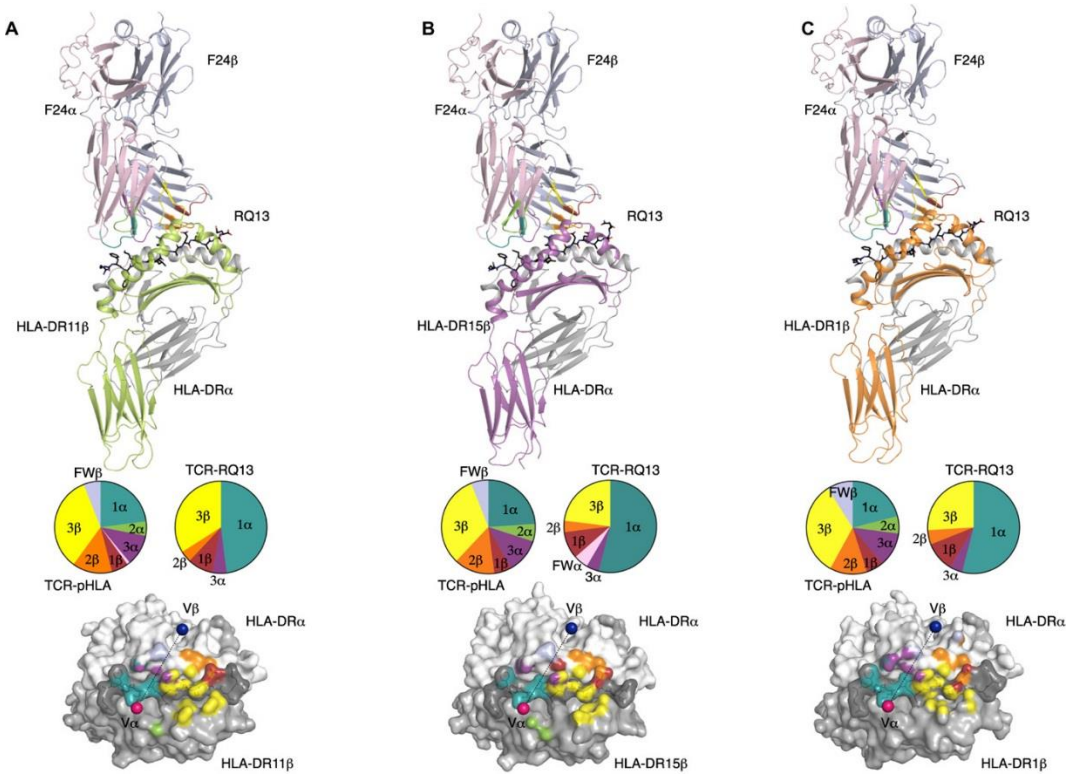

F24 TCR cross-recognition of the RQ13 epitope presented by multiple HLA-DR alleles.

Top: The F24 TCR (α chain in pale pink, and β chain in pale blue) recognizing RQ13 (black sticks) presented by HLA-DR11 (**A**), HLA-DR15 (**B**), and HLA-DR1 (**C**). The HLA-DR α chain is colored pale gray, whereas the β chains of HLA-DR11, HLA-DR15, and HLA-DR1 are shown in green, purple, and orange, respectively. The CDR1α, CDR2α, and CDR3α loops are shown in teal, green, and purple, whereas the CDR1β, CDR2β, and CDR3β loops are shown in red, orange, and yellow, respectively. Pie charts represent the contribution of each F24 TCR segments toward the peptide-HLA complex (left) or toward the peptide only (right) on HLA-DR11 (A), HLA-DR15 (B), and HLA-DR1 (C) presenting the RQ13 epitope. Bottom panels show the footprint of the F24 TCR on the surface of each HLA-DR–RQ13 complex. The colors correspond to each TCR segment involved in the contact according to the top panels; the magenta and blue spheres represent the center of mass for Vα and Vβ, respectively.

FIG 6

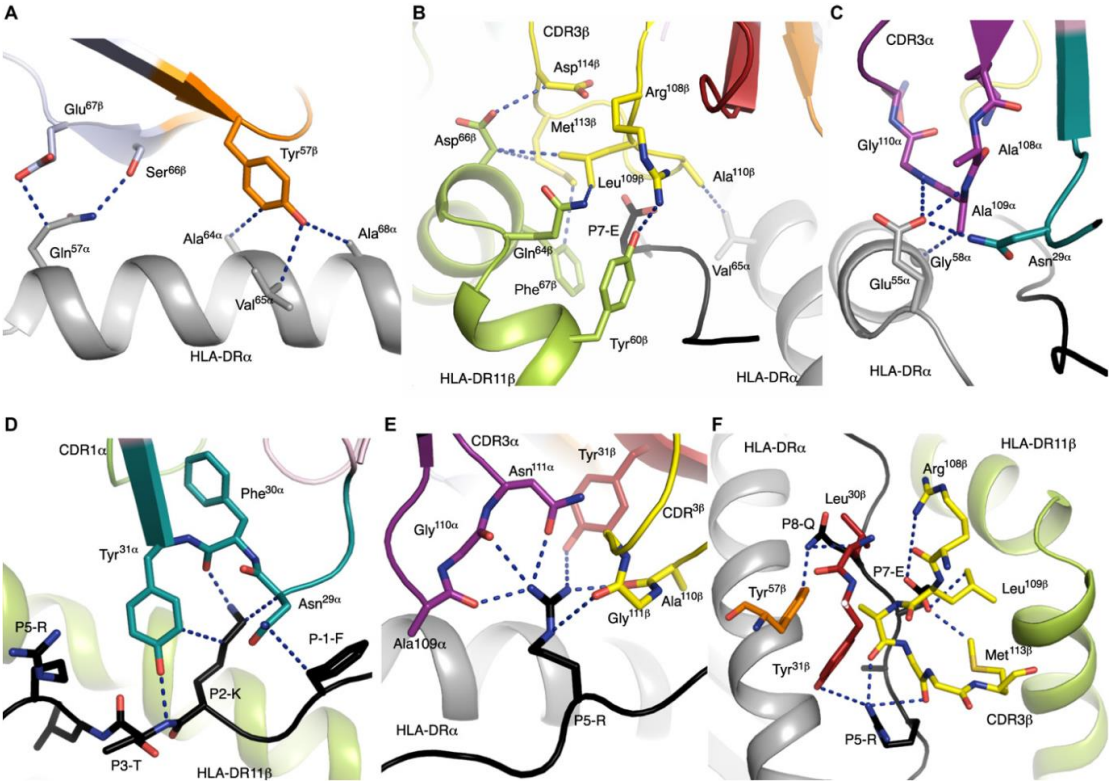

The F24 TCR recognition is primarily focused on the HIV epitope.

F24 TCR interactions with the HLA-DR11 chain (α chain in gray and β chain in green cartoon) (**A**) via the CDR2β loop (orange) and the F24 TCR β-chain framework (pale blue), (**B**) CDR3β residues (yellow), and (**C**) the CDR1α (teal) and CDR3α (purple) loops. Interactions of the RQ13 peptide (black sticks) (**D**) with F24 TCR CDR1α (teal), (**E**) the two CDR3 loops (α, purple; β, yellow), (**F**) CDR1β (red), CDR2β (orange), and CDR3β residues (yellow). The structures are shown in cartoon representation, interacting residues are depicted in sticks, and hydrogen bonds and van der Waals interactions are shown in blue dashed lines.

FIG 7

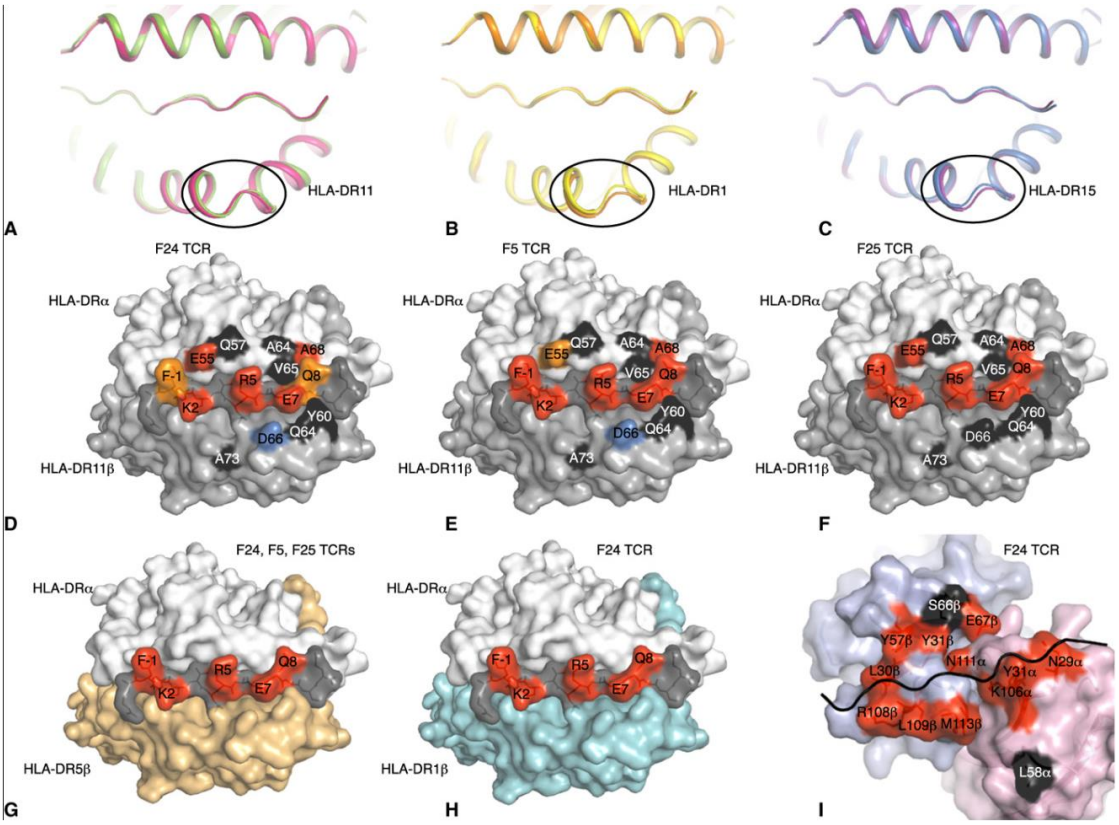

Antigen-binding cleft conformational changes, and energetic footprints of the public TCRs on the RQ13 peptide, in the context of multiple HLA-DR alleles.

Overlay of HLA-DR molecules in their free conformation in green, orange, and purple for HLA-DR11 (**A**), HLA-DR1 (**B**), and HLA-DR15 (**C**), respectively, with their F24 TCR-bound structure in pink, yellow, and blue, respectively. The RQ13 epitope is colored according to the bound HLA-DR molecule and represented as loop. The black circle highlights the hinge of the β-chain helix that changes conformation upon F24 TCR binding in HLA-DR1 (B) and HLA-DR15 (C) molecules. (**D** to **F**) Energetic footprint of F24 (D), F5 (E), and F25 (F) TCRs on the HLA-DR11–RQ13 complex. Energetic contribution determined by SPR, and the impact of each mutation was classified as no effect (<threefold affinity decrease, colored black), moderate (three- to fivefold affinity reduction, orange), critical (>fivefold affinity decrease, red), or improving the interaction (>threefold increase in affinity, blue). (**G** to **I**) The affinity of the TCR F24 mutants was determined by SPR. The RQ13 peptide is represented as black loop. The effect of each mutation is represented on the surface and colored as per the HLA-DR11 mutant in (D).

TABLE 1
Affinity measurements
Kd_{eq} is in μM; k_{on} is in M^{-1} s^{-1} × 10^4; k_{off} is in s^{-1}; $t_{1/2}$ is in s. ND, not determined. The error is representative of the SD of the experiment performed in duplicate from at least two independent experiments ($n \geq 2$).

Kd_{eq}	**DR1-Gag293***	**DR1-RQ13**	**DR11-Gag293***	**DR11-RQ13**	**DR15-Gag293**	**DR15-RQ13**	**DRB5-Gag293***	**DRB5-RQ13**
F24	6.97 ± 0.22	10.56 ± 2.62	0.86 ± 0.15	1.16 ± 0.48	5.09 ± 0.45	6.90 ± 0.62	2.58 ± 0.19	2.49 ± 0.80
F25	51.50 ± 3.00	153.4 ± 10.65	3.58 ± 0.25	5.36 ± 1.41	152.0 ± 15.56	159.6 ± 29.69	16.00 ± 0.60	37.28 ± 2.02
F5	>100	173.0 ± 9.90	11.06 ± 1.73	14.33 ± 3.18	122.0 ± 14.14	74.48 ± 13.34	74.45 ± 6.25	75.6 ± 4.53
k_{on}	**DR1-Gag293**	**DR1-RQ13**	**DR11-Gag293**	**DR11-RQ13**	**DR15-Gag293**	**DR15-RQ13**	**DRB5-Gag293**	**DRB5-RQ13**
F24	1.15 ± 0.54	1.28 ± 0.24	10.00 ± 0. 30	10.41 ± 0.79	4.95 ± 0.03	4.50 ± 0.05	5.29 ± 0.54	4.54 ± 0.09
F25	ND	ND	9.14 ± 1.36	5.42 ± 0.07	ND	ND	ND	0.21 ± 0.02
F5	ND	ND	1.51 ± 0.07	0.89 ± 0.03	ND	ND	ND	ND
k_{off}	**DR1-Gag293**	**DR1-RQ13**	**DR11-Gag293**	**DR11-RQ13**	**DR15-Gag293**	**DR15-RQ13**	**DRB5-Gag293**	**DRB5-RQ13**
F24	0.418 ± 0.013	0.172 ± 0.016	0.062 ± 0.002	0.050 ± 0.001	0.142 ± 0.006	0.153 ± 0.008	0.179 ± 0.009	0.167 ± 0.003
F25	ND	ND	0.253 ± 0.005	0.113 ± 0.004	ND	ND	ND	0.498 ± 0.076
F5	ND	ND	0.160 ± 0.045	0.107 ± 0.001	ND	ND	ND	ND
$t_{1/2}$	**DR1-Gag293**	**DR1-RQ13**	**DR11-Gag293**	**DR11-RQ13**	**DR15-Gag293**	**DR15-RQ13**	**DRB5-Gag293**	**DRB5-RQ13**
F24	1.6	4.0	11.1	11.8	4.8	4.5	3.8	4.1
F25	ND	ND	2.7	6.1	ND	ND	ND	1.4
F5	ND	ND	4.3	6.5	ND	ND	ND	ND

*Kd_{eq} values previously published (*10*).